right side of Fig. 3 the Coulomb gap continues to grow with increasingly positive V_g. For even larger gate voltages than shown in the figure (up to 40 V) the Coulomb gap exceeds 150 mV and there is no evidence for any more Coulomb oscillations.

This behaviour can be understood if electrons are being added to the valence band of the nanocrystal with increasingly positive V_g. In this case, for some sufficiently positive V_g, every state in the valence band is filled, and the next extended state of the nanocrystal lies in the conductance band, $2eV$ higher in energy. In this interpretation, the large gap at positive V_g corresponds to a completely filled valence band. Starting on the right side of Fig. 3 and decreasing V_g, the first Coulomb oscillation of Fig. 3 then corresponds to the removal of the first electron from, or alternatively the addition of the first hole to, the valence band. A further decrease in V_g adds additional holes. The addition energies for the second, third and fourth holes are $\Delta_2 = 14 \pm 2$ meV, $\Delta_3 = 29 \pm 3$ meV and $\Delta_4 = 22 \pm 2$ meV, as is indicated in Fig. 3c.

Note that in the Coulomb blockade model, the energy Δ_2, for adding the second hole to the nanocrystal is simply the Coulomb interaction, U, between holes, as the lowest-lying hole state is doubly degenerate. The energy, Δ_3, for adding the third hole, in contrast, is $U + \Delta E$, where ΔE is the difference between the ground and first excited single-particle state. The addition energy for the fourth hole, Δ_4, is again U because the first excited state is also doubly degenerate. The results given above are somewhat consistent with this scheme: for example, Δ_3, predicted to be $U + \Delta E$, is greater than Δ_2, which is predicted to be U.

Nevertheless, discrepancies remain. The energy for adding the second hole, $\Delta_2 = 14$ meV, is significantly smaller than the values of $U \sim 50$ mV obtained from simple electrostatic estimates or from measurements of other samples. In addition, the measured Δ_4 is greater than Δ_2, whereas in the Coulomb blockade model they should be the same. The origin of these differences remains unclear, although the effects of exchange and correlations are expected to be important for these few-hole systems. We also emphasize that the large gap at positive V_g has been seen in only one device. To confirm that this gap is associated with a filled valence band and to verify the inferred hole addition energies, it will be necessary to repeat these measurements on other samples.

This work represents a new type of spectroscopy for single nanocrystals. Unlike optical measurements, where electron–hole pairs are created, these measurements probe the energy for adding a single type of charge carrier. We hope that these results will stimulate new calculations of the hole addition energies for a CdSe nanocrystal that include the effects of exchange, correlations, and screening by the metallic electrodes. Future measurements will investigate how the ground-state and excited-state properties vary with the size, shape and composition of nanocrystals as well as with the composition of the leads. □

1. Brus, L. Quantum crystallites and nonlinear optics. *Appl. Phys. A* **53,** 465–474 (1991).
2. Alivisatos, A. P. Semiconductor clusters, nanocrystals, and quantum dots. *Science* **271,** 933–937 (1996).
3. Kastner, M. A. Artificial atoms. *Phys. Today* **46,** 24–31 (1993).
4. Ashoori, R. C. Electrons in artificial atoms. *Nature* **380,** 559 (1996).
5. Tarucha, S., Austing, D. G., Honda, T., van der Hage, R. J. & Kouwenhoven, L. P. Shell filling and spin effects in a few electron quantum dot. *Phys. Rev. Lett.* **77,** 3613–3616 (1996).
6. Kouwenhoven, L. P. & McEuen, P. L. in *Nanoscience and Technology* (ed. Timp, G.) (AIP Press, New York, in the press).
7. Colvin, V. L., Schlamp, M. C. & Alivisatos, A. P. Light-emitting diodes made from cadmium selenide nanocrystals and a semiconducting polymer. *Nature* **370,** 354–357 (1994).
8. Dabbousi, B. O., Bawendi, M. G., Onitsuka, O. & Rubner, M. F. Electroluminescence from CdSe quantum-dot/polymer composites. *Appl. Phys. Lett.* **66,** 1316–1318 (1995).
9. Greenham, N. C., Peng, X. & Alivisatos, A. P. Charge separation and transport in conjugated-polymer/semiconductor-nanocrystal composites studied by photoluminescence quenching and photoconductivity. *Phys. Rev. B* **54,** 17628–17637 (1996).
10. Alperson, B., Cohen, S., Rubinstein, I. & Hodes, G. Room-temperature conductance spectroscopy of CdSe quantum dots using a modified scanning force microscope. *Phys. Rev. B* **53,** 17017–17020 (1995).
11. Klein, D. L., McEuen, P. L., Bowen Katari, J. E. & Alivisatos, A. P. An approach to electrical studies of single nanocrystals. *Appl. Phys. Lett.* **68,** 2574–2576 (1996).
12. Andres, R. P. *et al.* Coulomb staircase at room temperature in a self-assembled molecular nanostructure. *Science* **272,** 1323–1325 (1996).
13. Sato, T. & Ahmed, H. Observation of a Coulomb staircase in electron transport through a molecularly linked chain of gold colloidal particles. *Appl. Phys. Lett.* **70,** 2579–2761 (1997).
14. Blanton, S. A., Dehestani, A., Lin, P. C. & Guyotsionnest, P. Photoluminescence of single semiconductor nanocrystallites by two-photon excitation microscopy. *Chem. Phys. Let.* **229,** 317–322 (1994).
15. Empedocles, S. A., Norris, D. J. & Bawendi, M. G. Photoluminescence spectroscopy of single CdSe nanocrystallite quantum dot. *Phys. Rev. Lett.* **77,** 3873–3876 (1996).
16. Nirmal, M. *et al.* Fluorescence intermittency in single cadmium selenide nanocrystals. *Nature* **383,** 802–804 (1996).
17. Ralph, D. C., Black, C. T. & Tinkham, M. Gate-voltage studies of discrete electronic states in aluminum nanoparticles. *Phys. Rev. Lett.* **78,** 4087–4090 (1997).
18. Bowen-Katari, J. E., Colvin, V. L. & Alivisatos, A. P. X-ray photoelectron spectroscopy of CdSe nanocrystals with applications to studies of the nanocrystal surface. *J. Phys. Chem.* **98,** 4109–4117 (1994).
19. Murray, C. B., Norris, D. B. & Bawendi, M. G. Synthesis and characterization of nearly monodisperse CdE (E = S, SE, TE) semiconductor nanocrystals. *J. Am. Chem. Soc.* **115,** 8706–8715 (1993).
20. Porter, M. D., Bright, T. B., Allara, D. L. & Chidsey, C. E. D. Spontaneously organized molecular assemblies. IV. Structural characterization of n-alkyl thiol monolayers on gold by optical ellipsometry, infrared spectroscopy, and electrochemistry. *J. Am. Chem. Soc.* **109,** 3559–3568 (1987).
21. Bain, C. D. *et al.* Formation of monolayer films by the spontaneous assembly of organic thiols from solution onto gold. *J. Am. Chem. Soc.* **111,** 321–335 (1989).
22. Boulas, C., Davidovits, J. V., Rondelez, F. & Vuillaumeume, D. Suppression of charge carrier tunneling through organic self-assembled monolayers. *Phys. Rev. Lett.* **76,** 4797–4800 (1996).
23. Ekimov, I. *et al.* Absorption and intensity-dependent photoluminescence measurements on CdSe quantum dots: assignment of the first electronic transitions. *J. Opt. Soc. Am.* **10,** 100–107 (1993).
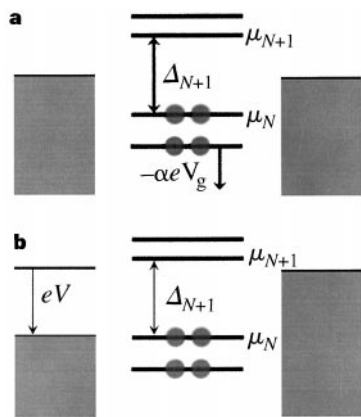
Figure 4 a, Energy-level diagram for a nanocrystal with N electrons at a gate voltage midway between two Coulomb oscillations. The electrochemical potential of the N-electron nanocrystal is denoted μ_N, and the electrochemical potential of the $(N + 1)$-electron nanocrystal is denoted μ_{N+1}. **b**, The application of a finite bias, V, can overcome the Coulomb gap. The maximal V applied before conduction occurs is equal to the addition energy, Δ_{N+1} for the $(N + 1)$th electron.

A tough SiAlON ceramic based on α-Si₃N₄ with a whisker-like microstructure

I-Wei Chen*† & Anatoly Rosenflanz*†

* *Department of Materials Science and Engineering, University of Michigan, Ann Arbor, Michigan 48109-2136, USA*

Silicon nitride (Si₃N₄) is a light, hard and strong engineering ceramic[1,2]. It can withstand harsh environments and support heavy loads at temperatures beyond those at which metals and polymers fail. It can also be manufactured reliably at a reasonable cost and in large quantities. There are two forms of silicon nitride[3]: α-Si₃N₄ and β-Si₃N₄. The former is harder, but only

† Present address: Department of Materials Science and Engineering, University of Pennsylvania, 3231 Walnut Street, Philadelphia, Pennsylvania 19104-6272, USA.

the latter is currently used in engineering applications, because only this form can be given a microstructure resembling a whisker-reinforced composite[1,2,4], which gives it the necessary toughness and strength. Here we report the synthesis of a tough α-Si$_3$N$_4$ solid solution with this kind of microstructure. This material is 40% harder than β-Si$_3$N$_4$ and is equally strong and tough. Its hardness (22 GPa) is exceeded only by boron carbide and diamond (which are both brittle). These properties mean that this form of α-Si$_3$N$_4$ should be preferred over β-Si$_3$N$_4$ for all engineering applications, and it should open up new potential areas in which the ceramic can be applied.

Si$_3$N$_4$ is inherently strong because of the covalent chemical bond between Si and N. α-Si$_3$N$_4$ has a structure similar to that of β-Si$_3$N$_4$, containing SiN$_4$ tetrahedra forming a corner-shared three-dimensional network with the characteristic (001) plane of a hexagonal structure[3]. This is also the plane of fast growth in β-Si$_3$N$_4$. The stacking of the planes is different in α and β structure; it is ABCD in α-Si$_3$N$_4$ and AB or CD in β-Si$_3$N$_4$. The longer stacking sequence in α-Si$_3$N$_4$ is responsible for its higher hardness because of the longer Burgers vector required for slip dislocations[5].

α-Si$_3$N$_4$ is unstable relative to β-Si$_3$N$_4$ and converts to the latter at higher temperature. This turns out to be useful. If α-Si$_3$N$_4$ is used as a starting powder and slowly converted to β-Si$_3$N$_4$ in the presence of a sintering, bonding liquid of silicon oxynitride, the newly grown crystals that consume the unstable matrix tend to take the shape of long rods in much the same way as crystals found in geological formations. The resultant β-Si$_3$N$_4$ has a microstructure that mimics a log-jam or pressed wood, but on a much finer scale. It contains hexagonal rods of single crystals as thin as several micrometres, bonded together and reinforcing each other. This makes β-Si$_3$N$_4$
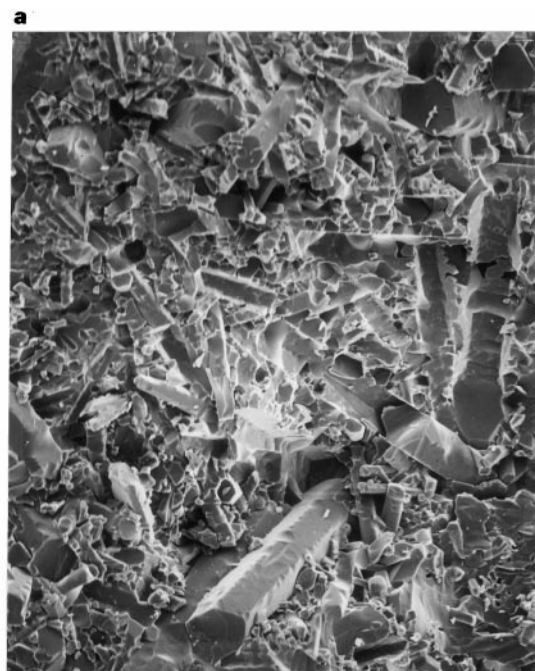

Figure 2 Fracture toughness (K_{1c}) and hardness (H_V) of Nd$_{0.4}$Si$_{9.9}$Al$_{2.1}$O$_{0.9}$N$_{15.1}$ (known as Nd-1209) samples with different amounts of α'-SiAlON; the remainder is untransformed β-Si$_3$N$_4$. Both properties increase with the amount of $\beta \rightarrow \alpha'$ transformation. Using the nomenclature described in the text, $m = 1.2$ and $n = 0.9$ in Nd-1209.
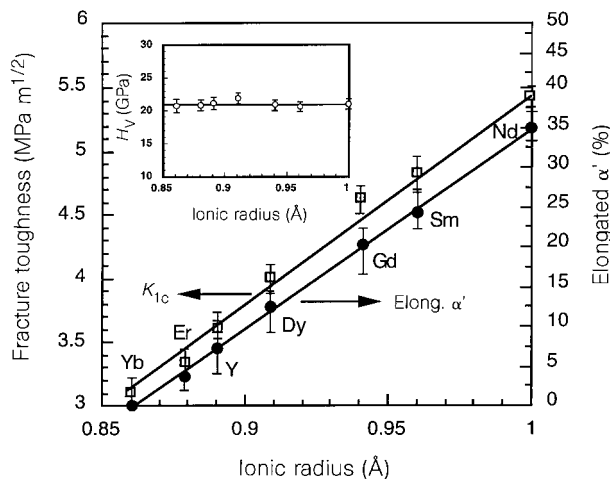

Figure 1 Properties of an Nd$_{0.4}$Si$_{9.9}$Al$_{2.1}$O$_{0.9}$N$_{15.1}$ sample. **a**, Scanning electron micrograph of a fracture surface showing elongated grains. **b**, X-ray diffraction pattern of **a** showing single-phase α'-SiAlON reflections ($a = 7.8140$ Å, $c = 5.6914$ Å). Fired at 1,950 °C for 1.5 h.

Figure 3 Fracture toughness (K_{1c}) and amount of elongated grains of seven α'-SiAlONs stabilized by cations of different ionic radii for an overall composition of R$_{0.4}$Si$_{9.6}$Al$_{2.4}$O$_{1.2}$N$_{14.8}$ ($m = 1.2, n = 1.2$; see text). The amount of elongated α' grains was measured by stereology (that is, by counting their projected areas on the photograph of the fracture surface). The inset shows a nearly constant hardness (H_V) value for all samples.

difficult to break, hence its higher strength and toughness. We have known for 30 years that if β-Si$_3$N$_4$ is used as a starting powder, it is difficult to obtain the above microstructure and the high strength and toughness[4,6,7]. Indeed, without the whisker-like microstructure, high toughness and high strength would be very difficult to achieve in any covalent ceramic[8], even though it may possess extraordinary hardness and oxidation resistance[9,10].

Can the same microstructure be obtained for α-Si$_3$N$_4$, or its cation-stabilized solid solution known as α'-SiAlON? This solid-solution has a general formula M$_{m/z}$Si$_{12-m-n}$Al$_{m+n}$O$_n$N$_{16-n}$ where M is a cation of charge z that enters the large interstitial site available in α-Si$_3$N$_4$ (ref. 11). Crystallographically, the hexagonal (001) plane and the prismatic (210) plane have essentially the same atomic structures in both α- and β-Si$_3$N$_4$. Therefore, the growth habit and the microstructure should be similar. Nevertheless, despite numerous attempts to produce α'-SiAlON with a whisker-like microstructure, few have succeeded and none have reported improved fracture toughness[12–18]. For example, after a systematic study of α'-SiAlONs, Nordberg et al.[18] recently concluded that "no systematic variation of mechanical properties with the overall size and shape of the α'-SiAlON grains could be discerned". They also found liquid-rich compositions promoting the formation of elongated α'-SiAlON grains[17]. This, however, is undesirable because of the poor mechanical and chemical stability of the liquid-rich SiAlONs at high temperature[1,2].

It is notable that in all the previous studies only α-Si$_3$N$_4$ was used as starting material. On the other hand, the fact that self-reinforced β-Si$_3$N$_4$ composed of elongated crystals can be readily obtained by using α-Si$_3$N$_4$ as a starting powder suggests that the reverse scheme (using β-Si$_3$N$_4$ as a starting powder) could be successful if self-reinforced α'-SiAlON is to be obtained. This is indeed the case, as illustrated by the following examples.

We prepared samples of Nd-stabilized α'-SiAlON using β-Si$_3$N$_4$ powder (SNP21FC, Denka Inc.; the powder contains 7% α-Si$_3$N$_4$). The microstructure contains many elongated grains with sharp, crystallographic facets (Fig. 1a). The X-ray diffraction pattern of this specimen (Fig. 1b) confirms that only reflections of α'-SiAlON exist. This material is both hard and tough, with an indentation

Table 1 Properties of Yb$_{0.4}$Si$_{9.6}$Al$_{2.4}$O$_{1.2}$N$_{14.8}$ fired in three different ways

Firing	Elongated α' (%)	H_V (GPa)	K_{1c} (MPa m$^{1/2}$)
A	0	20.8 ± 0.3	3.1 ± 0.3
B	20	21.1 ± 0.8	4.8 ± 0.4
C	25	21.4 ± 0.5	5.1 ± 0.4

H_V, hardness; K_{1c}, fracture toughness; see text for description of firings A, B and C.
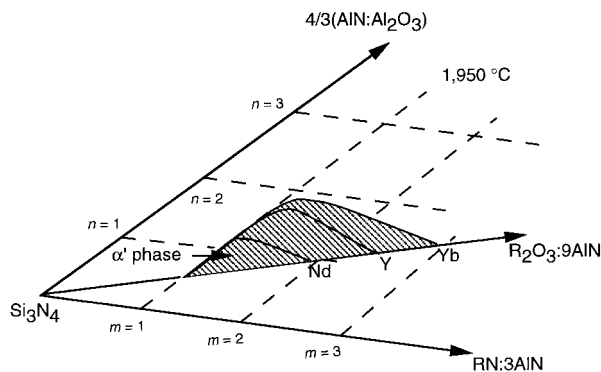

Figure 4 α' phase region in the Si$_3$N$_4$ corner of the phase diagram of (Si, Al, R) (N, O) system at 1,950 °C (ref. 21). It is smaller for larger stabilizing cations and lower temperatures. m and n are defined in the text; R is the rare-earth stabilizing element.

hardness of 21.7 GPa and an indentation toughness of 6.3 MPa m$^{1/2}$. Using identical measuring methods, a self-reinforced β-Si$_3$N$_4$ showed a hardness of 15.5 GPa and a toughness of 6.2 MPa m$^{1/2}$. Thus, the self-reinforced α'-SiAlON is 40% harder than β-Si$_3$N$_4$ and is equally tough. In comparison, a variety of equiaxed α'-SiAlONs made from α-Si$_3$N$_4$ powder showed a typical hardness ranging from 20.5 to 22.0 GPa and a toughness of 3.0 MPa m$^{1/2}$. The three-point bend strengths of the self-reinforced α'-SiAlON samples exceeded 700 MPa, comparable to those of self-reinforced β-Si$_3$N$_4$ prepared in our laboratory but twice the values of α'-SiAlON made from α-Si$_3$N$_4$ powder. Also, compared with SiC (another engineering ceramic), the new α'-SiAlON is as hard but has improved strength and toughness.

The conversion from β-Si$_3$N$_4$ to α'-SiAlON is relatively slow in the above material. We followed the conversion in different samples and found it to have a direct effect on the properties. As shown in Fig. 2, there is a monotonic increase in both hardness and toughness with the amount of α'-SiAlON. The increase in hardness with the amount of α'-SiAlON is well known[19,20]. However, all previous reports[19,20] have indicated that the toughness decreases with the amount of α'-SiAlON. As the only difference between our materials and those studied in the past lies in the microstructure, the reason our materials behave differently is that the α'-SiAlON grains grown here are all elongated.

Elongated grains in β-Si$_3$N$_4$ are thought to form because of slow nucleation[7]. When α-Si$_3$N$_4$ powder is used to make β-Si$_3$N$_4$, only a small number of β-Si$_3$N$_4$ grains initially exist or are subsequently nucleated. These relatively few grains can then grow considerably in the (001) direction before they run into each other. Presumably, the same applies to the $\beta \rightarrow \alpha'$ transformation when β-Si$_3$N$_4$ powder is used. However, the formation of elongated α' grains is not always guaranteed by using β-Si$_3$N$_4$ powder. When the composition favours the formation of α'-SiAlON so much that the conversion of β-Si$_3$N$_4$ is too fast, the α'-SiAlON obtained still has fine equiaxed grains. This may be attributed to the overabundance of nucleation. An illustration of this trend is seen by comparing R$_{0.4}$Si$_{9.6}$Al$_{2.4}$O$_{1.2}$N$_{14.8}$ compositions using different rare earths (R). At 1,950 °C, all of these compositions yield 100% α'-SiAlON. Yet the microstructures of these samples are different, ranging from equiaxed grains (R is Yb) to elongated grains (R is Nd). Figure 3 shows their hardness and toughness, along with the percentage of elongated α'-grains. Obviously, only the amount of elongated α'-SiAlON is responsible for the toughness enhancement.

The systematic difference in the microstructure of different rare-earth-stabilized α'-SiAlONs is related to their phase stability. According to the phase diagram[21] shown in Fig. 4, the α'-region of Yb-α' is much larger than that of Nd-α' at the same temperature. Thus, Yb-α'-SiAlON is more stable and the driving force of $\beta \rightarrow \alpha'$ transformation is higher. This results in a higher nucleation rate and a finer grain size. This different phase stability is no doubt related to the ionic size of the stabilizing cations, as recently verified by molecular-orbital calculations[22].

If overabundance of nucleation is the problem, it should be possible to circumvent it by reacting at a lower temperature that provides slower kinetics and lower driving force[21]. In the Yb$_{0.4}$Si$_{9.6}$Al$_{2.4}$O$_{1.2}$N$_{14.8}$ composition, for example, we effected slower nucleation of α'-SiAlON by first holding it at 1,550 °C for 1.5 h (material B). This contrasts with the fine equiaxed grains obtained after direct firing at 1,950 °C (material A). Likewise, if the same composition is held at 1,650 °C for 12 h, the conversion to α'-SiAlON is also slowed and the final microstructure consists of elongated grains (material C). The properties of these three materials of identical compositions but different processing steps are summarized in Table 1 and show that, by controlling α' nucleation, very substantial enhancement of toughness can be achieved for Yb-α'-SiAlON. These Yb-α'-SiAlONs are extremely stable. For example, after holding at 1,500 °C for 240 h, the X-ray diffraction patterns

of these materials show only α′-SiAlON reflections in a pattern identical to that obtained before the treatment of 1,500 °C. Using other similar ways of controlling nucleation, we have been able to obtain high-toughness single-phase α′-SiAlON with rare-earth or Y stabilizer over a broad range of compositions[21]. □

1. Chen, I.-W., Becher, P. F., Mitomo, M., Petzow, G. & Yen, T.-S. *Silicon Nitride Ceramics* (Mater. Res. Soc., Pittsburgh, PA, 1993).
2. Hoffman, M. J. & Petzow, G. *Tailoring of Mechanical Properties of Si₃N₄ Ceramics* (Kluwer Academic, Dordrecht, 1994).
3. Hardie, D. & Jack, K. H. Crystal structure of silicon nitride. *Nature* **180**, 332–322 (1957).
4. Lange, F. F. Relations between strength, fracture energy, and microstructure of hot pressed Si₃N₄. *J. Am. Ceram. Soc.* **56**, 518–522 (1973).
5. Lewis, M. H., Fung, R. & Taplin, D. M. R. Indentation plasticity and fracture of Si₃N₄ ceramic alloys. *J. Mater. Sci.* **16**, 3437–3446 (1981).
6. Coe, R. F. Silicon nitride products. British Patent No. 1,092 637 (1967).
7. Lange, F. F. Fracture toughness of Si₃N₄ as a function of the initial α-phase content. *J. Am. Ceram. Soc.* **62**, 428–430 (1979).
8. Becher, P. F. Microstructure design of toughened ceramics. *J. Am. Ceram. Soc.* **74**, 255–269 (1991).
9. Riedel, R., Kleebe, H.-J. & Schonfelder, H. A covalent micro/nanocomposite resistant to high temperature oxidation. *Nature* **374**, 526–528 (1995).
10. Riedel, R. *et al.* A silicoboron carbonitride ceramic stable to 2,000 °C. *Nature* **382**, 796–786 (1996).
11. Hampshire, S., Park, H. K., Thompson, D. P. & Jack, K. H. α′-SiAlON ceramics. *Nature* **274**, 880–882 (1978).
12. Hwang, C. J., Susintzky, D. W. & Beaman, D. R. Preparation of multication α′-SiAlON containing strontium. *J. Am. Ceram. Soc.* **78**, 588–592 (1995).
13. Wang, H., Cheng, Y.-B., Muddle, B. C., Gao, L. & Yen, T. S. Preferred orientation in hot-pressed Ca α′SiAlON ceramics. *J. Mater. Sci. Lett.* **15**, 1447–1449 (1996).
14. Shen, Z., Ekström, T. & Nygren, M. Temperature stability of samarium-doped α′-SiAlON ceramics. *J. Eur. Ceram. Soc.* **16**, 43–53 (1996).
15. Shen, Z., Ekström, T. & Nygren, M. Ytterbium stabilized α′-SiAlON ceramics. *J. Phys. D* **296**, 893–904 (1996).
16. Shen, Z., Ekström, T. & Nygren, M. Homogeneity region and thermal stability of neodymium-doped α′-SiAlON ceramics. *J. Am. Ceram. Soc.* **79**, 721–732 (1996).
17. Shen, Z., Nordberg, L.-O., Nygren, M. & Ekström, T. in *Proc. Nato AST Engineering Ceramics '96— Higher Reliability through Processing* (ed. Babini, G. N.) 169–178 (Kluwer Academic, Dordrecht, 1997).
18. Nordberg, L.-O., Shen, Z., Nygren, M. & Ekström, T. On the extension of the α′-SiAlON solid solution range and anisotropic grain growth in Sm-doped α′-SiAlON ceramics. *J. Eur. Ceram. Soc.* **17**, 575–580 (1997).
19. Cao, G. Z. & Metselaar, R. α′-SiAlON ceramics, a review. *Chem. Mater.* **3**, 242–252 (1991).
20. Ekström, T. & Nygren, M. SiAlON ceramics. *J. Am. Ceram. Soc.* **75**, 259–276 (1992).
21. Rosenflanz, A. α′-SiAlON: Phase stability, phase transformations and microstructural evaluations. Thesis, Univ. Michigan (1997).
22. Nakayasu, T., Yamada, T., Tanaka, I., Adachi, H. & Goto, S. Electronic structures of Ln³⁺ α′-SiAlONs with correlations to solubility and solution effects. *J. Am. Ceram. Soc.* **79**, 2527–2532 (1996).

Synthesis of microporous transition-metal-oxide molecular sieves by a supramolecular templating mechanism

Tao Sun & Jackie Y. Ying

Department of Chemical Engineering, Massachusetts Institute of Technology, Cambridge, Massachusetts 02139-4307, USA

....

Mesoporous bulk[1–4] and thin-film[5–7] silicates with pore sizes of 20–100 Å can be synthesized by using micellar aggregates of long-chain organic surfactant molecules as templates to direct the structure of the silicate network. Because of the potential applications of these molecular-sieve materials as catalysts, separation membranes and components of sensors, it is desirable to extend the range of accessible pore sizes and material compositions. Mesoporous oxides in which transition metals partially[8] and fully[9–13] substitute for silicon have been made by similar means, in the latter case by ensuring strong interactions between the surfactants and the transition-metal alkoxide precursors. Templating with organic molecules has also been long used for the synthesis of microporous materials—synthetic zeolites—which have smaller pore sizes (4–15 Å), but here the organic molecules are shorter-chain amphiphiles which are too small to be considered true surfactants and so act as discrete entities around which the framework crystallizes[14–16]. Here we show that even such short-chain molecules can aggregate into supramolecular templates when they form bonds with transition-metal (niobium) alkoxides, and that in this way they can direct the formation of transition-metal oxides with pore sizes of less than 20 Å. These pore sizes, which result from the smaller diameter of micellar structures of the short-chain amines relative to the longer-chain surfactants used for the synthesis of mesoporous materials, qualify the resulting molecular sieves as microporous, even though the supramolecular templating mechanism is similar to that used to make the mesoporous materials. Thus our approach extends the supramolecular templating method to afford microporous transition-metal oxides.

In a typical synthesis, 3 g of $Nb(OC_2H_5)_5$ was hydrolysed in 41 g of deionized water to give a suspension of loosely bound niobium oxy-alkoxide precipitates. 0.96 g of hexylamine was then introduced as a templating agent to form an organic–inorganic nanocomposite. The nanocomposite was hydrothermally treated to promote condensation and crystallization. The aged product was recovered by filtration and dried at room temperature. Figure 1 shows the X-ray diffraction (XRD) patterns of niobium oxide–hexylamine nanocomposites produced by different ageing temperatures. For comparison, a product prepared by direct hydrolysis of niobium ethoxide without the addition of hexylamine was examined. Figure 1, trace a, shows that the material prepared without a templating agent was amorphous, having no distinct XRD peaks. With hexylamine addition, a broad, low-intensity (100) diffraction peak was found after ageing the material at ambient conditions for 24 hours (Fig. 1 trace b). After the ageing temperature was raised to
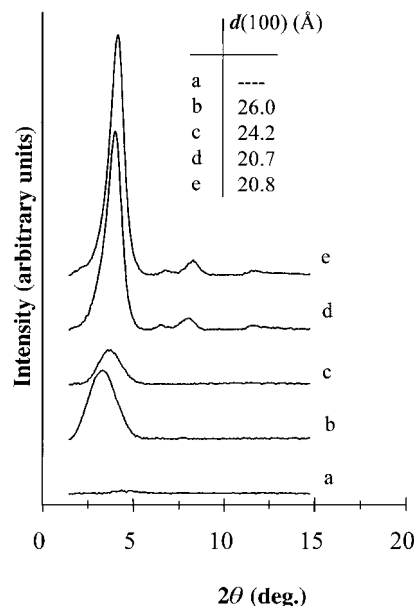
	$d(100)$ (Å)
a	----
b	26.0
c	24.2
d	20.7
e	20.8

Figure 1 X-ray diffraction (XRD) patterns of as-prepared niobium oxide samples derived from hydrolysis of $Nb(OC_2H_5)_5$. Trace a, sample prepared without amine templating agent; traces b–e, samples prepared with subsequent hexylamine addition (Nb : amine molar ratio of 1 : 0.75). The samples were examined after ageing at 25 °C for 24 h (a, b), 96 °C for 24 h (c), 180 °C for 24 h (d), and 180 °C for 48 h (e). The XRD patterns were obtained with a Siemens D5000 θ–θ diffractometer with CuKα radiation (λ = 1.5418 Å).